ACS Partner Journal

Journal of the American Society for Mass Spectrometry

pubs.acs.org/jasms

Research Article

A New Strategy Coupling Ion-Mobility-Selective CID and Cryogenic IR Spectroscopy to Identify Glycan Anomers

Robert P. Pellegrinelli, Lei Yue, Eduardo Carrascosa, Ahmed Ben Faleh, Stephan Warnke, Priyanka Bansal, and Thomas R. Rizzo*

Cite This: *J. Am. Soc. Mass Spectrom.* 2022, 33, 859−864

Read Online

ACCESS | Metrics & More | Article Recommendations | Supporting Information

ABSTRACT: Determining the primary structure of glycans remains challenging due to their isomeric complexity. While high-resolution ion mobility spectrometry (IMS) has recently allowed distinguishing between many glycan isomers, the arrival-time distributions (ATDs) frequently exhibit multiple peaks, which can arise from positional isomers, reducing-end anomers, or different conformations. Here, we present the combination of ultrahigh-resolution ion mobility, collision-induced dissociation (CID), and cryogenic infrared (IR) spectroscopy as a systematic method to identify reducing-end anomers of glycans. Previous studies have suggested that high-resolution ion mobility of sodiated glycans is able to separate the two reducing-end anomers. In this case, Y-fragments generated from mobility-separated precursor species should also contain a single anomer at their reducing end. We confirm that this is the case by comparing the IR spectra of selected Y-fragments to those of anomerically pure mono- and disaccharides, allowing the assignment of the mobility-separated precursor and its IR spectrum to a single reducing-end anomer. The anomerically pure precursor glycans can henceforth be rapidly identified on the basis of their IR spectrum alone, allowing them to be distinguished from other isomeric forms.

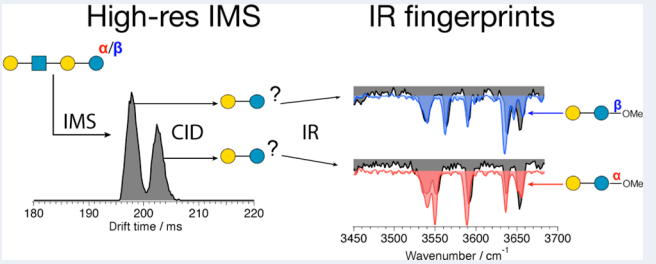

KEYWORDS: *ion mobility, ion spectroscopy, mass spectrometry, glycan analysis, isomers*

INTRODUCTION

Glycans play a central role in many biological processes, including protein folding, cellular signaling, and recognition of pathogens by the immune system.[1−3] The SARS-CoV-2 spike protein, for example, has a number of N-linked and O-linked glycans that both contribute to its folding as well as help shield it from immune detection.[4−9] Despite the importance of glycan structure, the intrinsic isomeric complexity of glycans makes primary sequence determination challenging. Many of the monosaccharide building blocks are isomers, making them indistinguishable by their mass. Moreover, they can link together at different positions, resulting in regioisomers and branched structures. Finally, the glycosidic linkage that forms at the anomeric carbon can exist either in an α- or β-configuration, and glycans with a free reducing-end OH can undergo mutarotation at the anomeric carbon in solution.

Techniques for glycan analysis, although rapidly developing, do not yet provide a comprehensive solution for deciphering their structure. Tandem mass spectrometry (MS^n) is currently the most widely used approach for glycan sequencing and analysis due to its speed and sensitivity.[10−12] This technique has recently unraveled many structural details such as linkage position, branching, and in some cases the anomericity of small glycans.[13−16]

Combining other analytical techniques with MS^n greatly expands its capability to analyze glycan structure. For example, coupling MS^n with liquid chromatography gives rise to a powerful analytical tool, which when combined with enzymatic digestion can be used to fully sequence even large oligosaccharides.[17−19] Although powerful, these techniques often require chemical modification, long incubation times, and multiple chromatographic runs, making them complex and time-consuming.

Ion mobility spectrometry (IMS), a technique in which gas-phase ions are separated based on their collisional cross section with an inert buffer gas, has been combined with MS^n to provide a rapid and effective tool for glycan analysis.[20−22] Such studies in which fragments generated by collision-induced dissociation (CID) are characterized by IMS have led to the identification of regioisomers and anomers of the precursor glycans.[23,24] Ultrahigh-resolution IMS has been able to separate subtle substructures in small glycans,[25−30] and a

Received: February 10, 2022
Revised: April 7, 2022
Accepted: April 7, 2022
Published: April 19, 2022

cyclic IMS instrument has recently been used to separate and partially identify the isomers of a set of pentasaccharides based on their fragmentation pattern.[28,29] However, the ever-increasing resolution of IMS devices leads to the observation of multiple peaks in the arrival-time distribution (ATD). This complicates the interpretation of IMS data, as the separated reducing-end anomers, which are in equilibrium in solution, can then be confused with other structures such as positional isomers, regioisomers, or conformers. For this reason, IMS−MS studies alone have difficulties identifying all the mobility-separated isomers unambiguously.

Infrared (IR) spectroscopy, on the other hand, is a technique that is sensitive to the most minute structural details of a molecule. While infrared multiple-photon dissociation (IRMPD) at ambient temperature has been used to identify the epimers and anomers of small glycans and their fragments,[23,31,32] cryogenic IR spectroscopy has enabled the fingerprinting of glycans of increasing size and isomeric complexity,[33−38] where the low temperatures of the analyte ions greatly enhance spectroscopic resolution by eliminating thermal inhomogeneous broadening.[39] Combining such techniques with ultrahigh-resolution IMS can be used to identify minor structural differences including positional isomers, even in glycans containing up to 10 monosaccharides.[36−38,40,41] Nevertheless, the vast number of possible structures makes it challenging to interpret complex vibrational spectra of larger oligosaccharides and determine their specific isomeric forms. Moreover, the size of most glycans puts them out of reach of current theoretical methods that are sometimes used to associate vibrational bands to a certain structure.[42,43] This problem can be overcome by using a database of spectral fingerprints constructed using glycan standards,[36,40] although analytical standards of pure isomeric forms are often expensive to produce or simply not available.

Breaking down glycans into smaller fragments by CID prior to spectroscopic investigation can simplify the interpretation of the spectra. This approach relies on breaking the molecule of interest into C- or Y-type fragments,[44] which are themselves intact glycans, and then matching their IR spectra to a database of known standards. This technique has recently revealed that for alkali-metal complexed C-type fragments, the anomericity of the glycosidic linkage is retained.[23,31,45,46] However, many glycosidic linkages preferentially produce B- or Y-type fragments, and this is a limiting factor to using only C-type fragments to sequence glycan structure. We have previously shown how Y-fragments can help identify glycan positional isomers.[41] In this work, we explore how Y-fragments, which carry the anomeric OH, can be used to distinguish and assign the reducing-end anomers from a set of mobility-separated oligosaccharides, thus allowing them to be distinguished from other isomeric forms in a sample. We propose a systematic approach, combining mobility-selective CID and cryogenic IR spectroscopy, which can identify the anomers of oligosaccharides using only a small set of anomerically pure and commercially available mono- and disaccharide standards. The spectra of the precursor molecules can then be assigned to a single anomer and added to a database, providing a spectral library of complex molecules for which anomerically pure standards are not available.

EXPERIMENTAL APPROACH

A newly developed instrument that combines ultrahigh-resolution ion mobility with CID and cryogenic infrared (IR) spectroscopy was used to perform the experiments presented in this work, and its details and characterization have been described recently.[47] Briefly, ions are generated by nanoelectrospray ionization (nESI) and guided by ion funnels into an ion mobility module, which uses structures for lossless ion manipulations (SLIM), implemented by a pair of mirror-image printed circuit boards (PCBs) as originally developed by Smith and co-workers.[25,26,48,49] Ions are accumulated in the first part of the SLIM device and then released as pulses onto a serpentine mobility path. They are driven through the 10 m long separation region by a traveling wave (TW) and separated based on their collisional cross section (CCS) with nitrogen, the pressure of which is maintained at 2.2 mbar. This IMS device features a resolving power of approximately 200 after a single separation cycle and reaches a resolution of 1000 after approximately 20 separation cycles.[47] Mobility-separated ions leaving the IMS region are guided through differentially pumped stages to a cryogenic, planar, multipole trap maintained at 45 K and a pressure of approximately 10^{-6} mbar. Accelerating the ions into the trap by increasing the difference in DC bias potential between the ion guides and the trap results in fragmentation by CID, and the fragments as well as precursor ions are detected by a reflectron time-of-flight mass spectrometer (ToF-MS).

The different mobility-separated precursors as well as their respective fragments can be identified by IR messenger tagging spectroscopy, which is performed in the ion trap. During a trapping cycle, the ions are collisionally cooled by an 80/20 He/N_2 gas mixture and tagged by weakly bound nitrogen molecules. A continuous-wave fiber-pumped IR laser (IPG, USA) operated at an output power of either 0.5 or 1 W irradiates the contents of the trap, and when the photon energy is in resonance with a vibrational transition in the molecular ion, the photon is absorbed and results in the loss of the nitrogen tag, which is detected as a decrease in the tagged ion signal and an increase in the untagged ion signal. A cryogenic infrared spectrum is obtained by plotting the ratio of the tagged ion signal to the sum of the tagged and untagged ion signal as a function of laser wavenumber.

Isotopic Labeling. The reducing-end OH of maltopentaose was isotopically labeled with ^{18}O by dissolving it in $H_2{}^{18}O$ for 1 week. This allowed the distinction of otherwise isomeric reducing and non-reducing-end fragments, which were investigated using a commercial Waters QToF Premier at 40 eV collision energy.

Materials. The oligosaccharides galacto-N-biose (Galβ1−3GalNAc) and maltopentaose were purchased from Carbosynth (UK). The tetrasaccharide lacto-N-neotetraose (LNnT) was purchased from Dextra (UK). The disaccharides methyl-α-lactoside, methyl-β-lactoside, methyl-α-maltosidase, and methyl-β-maltosidase were purchased from Synthose (Canada). Oxygen-18-labeled water, 97 atom % ^{18}O was purchased from abcr, Germany. All samples were used without further purification and diluted in a 50:50 water−methanol solution to a concentration of 10−50 μM. Only the singly sodiated cations were investigated in this work. All gases were 99.9999% purity.

RESULTS AND DISCUSSION

Identifying IMS-Separated Species of a Disaccharide. The singly sodiated disaccharide galacto-N-biose (Galβ1−3GalNAc), a core structure of mucin-type O-glycans,[50] showed only one major feature in its ATD, even after five cycles (~50

https://doi.org/10.1021/jasms.2c00043
J. Am. Soc. Mass Spectrom. 2022, 33, 859−864

m drift path) through the SLIM IMS device (Figure 1a). Two low-abundance structures appearing at 533 and 539 ms were also separated, but their IR spectra (Figure S1) show no resemblance to that of the main peak, suggesting that these are conformers that differ significantly in structure, possibly due to an open-ring form of the reducing-end GalNAc. However, further study of these species by fragmentation was not attempted due to their low abundance.

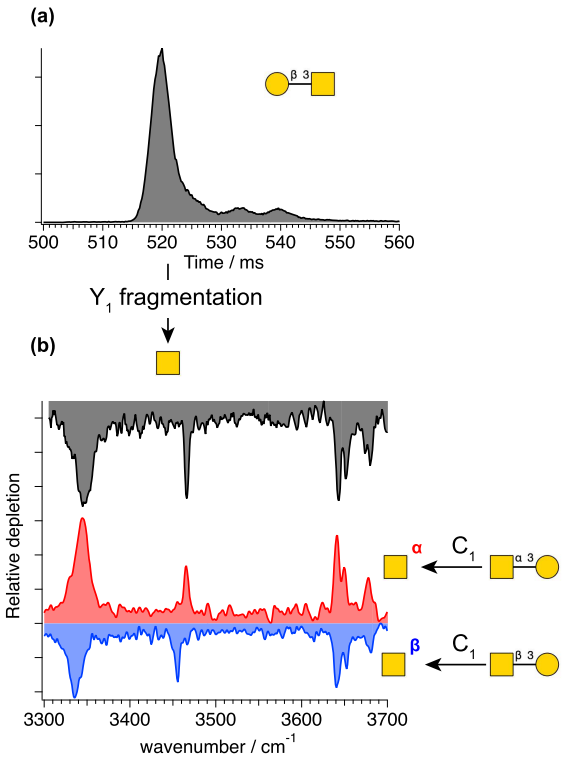

Figure 1. (a) Arrival-time distribution of the sodiated disaccharide Gal(β1−3)GalNAc after five separation cycles. (b) Comparison of the IR spectrum of the Y_1-fragment generated from the major mobility peak to that of the pure α- and β-anomers of GalNAc, produced by C_1 fragmentation from the disaccharides GalNAc(α-3)Gal and GalNAc-(β-3)Gal. In this and subsequent figures, the spectrum of the α-anomer is in red, and that of the β-anomer is in blue.

The Y_1-fragment from the major mobility peak was generated, and its vibrational spectrum was compared to those of anomerically pure standards (Figure 1b). The anomerically pure monosaccharides α-GalNAc and β-GalNAc were produced by C_1 fragmentation of the disaccharides GalNAc-Gal and GalNAc(β-3)Gal, respectively, in which the anomericity of the glycosidic bond is retained.[46] The spectrum of the Y_1-fragment matches that of the anomerically pure α-GalNAc, with all the bands appearing in the same positions with the same relative intensities. This identifies the major peak in the ATD of Figure 1a to be the α-reducing-end anomer of the precursor disaccharide Galβ1−3GalNAc. Given that mutarotation does not occur in the gas phase,[51] this suggests that the precursor disaccharide exists primarily in the α-configuration under the solution conditions studied. The IR fingerprint spectrum of the disaccharide was measured (Figure S1) and can be used to identify it in subsequent investigations.

Tetrasaccharide LNnT. In contrast to the example above, the human milk tetrasaccharide LNnT separates into two well-resolved peaks after two cycles on our ion mobility device (Figure 2a). Such bimodal distributions are commonly observed in ion mobility studies of reducing sugars, and it has been speculated, and in some cases confirmed, that they arise from a mixture of α- and β-reducing-end anomers.[27,28,37,51] To determine if the separated peaks in the ATD of Figure 2a indeed represent the reducing-end anomers and if so to assign them, we produce the Y_2-fragments (corresponding to lactose) from the mobility-separated precursor ion and compare their spectra to those of anomerically pure methyl-α-lactoside and methyl-β-lactoside (Figure 2b), which are locked into a single anomer at the reducing end by O-methylation.[31,51]

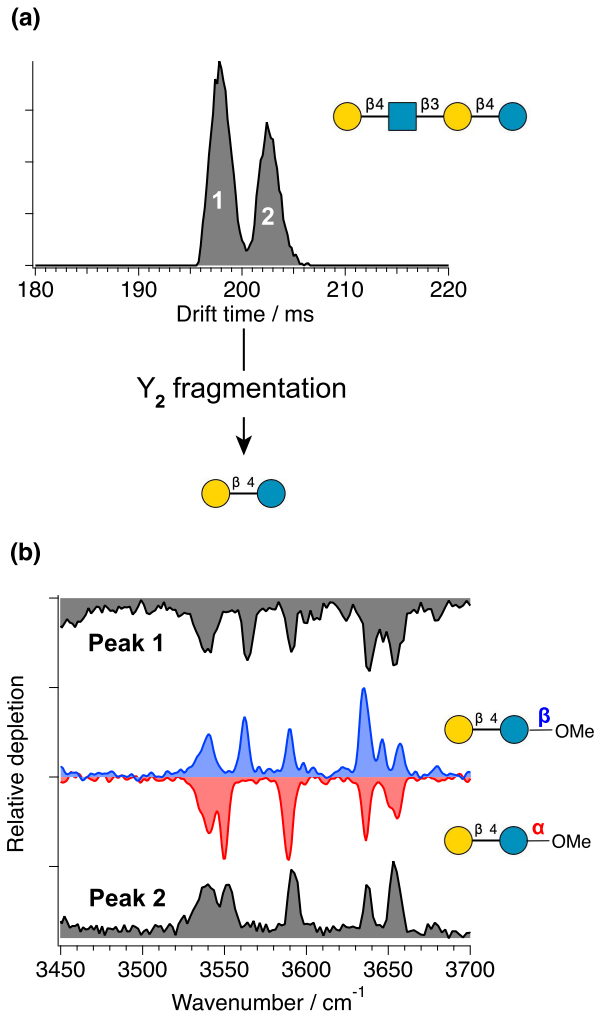

Figure 2. (a) Mobility separation of the precursor [LNnT + Na]$^+$ after two separation cycles (21 m drift path). (b) IR spectra of the Y_2-fragment (lactose) generated from the first and second mobility-separated precursors (gray) compared to those of methyl-β-lactoside (blue) and methyl-α-lactoside (red).

The IR spectra of the Y_2-fragments generated from each mobility peak are clearly distinguishable from each other, and each resembles one of the O-methylated standards, which allows us to identify the reducing anomers. The absence of the anomeric OH in the standards accounts for the slightly different absorption patterns observed in the 3630 to 3670 cm^{-1} region compared to the Y_2-fragments. Moreover, the slight shifts in the band positions can be attributed to differences in the hydrogen bonding network resulting from

https://doi.org/10.1021/jasms.2c00043
J. Am. Soc. Mass Spectrom. 2022, 33, 859−864

methylating the OH at the anomeric carbon. Nevertheless, the comparison between the spectra of the Y_2-fragments and the individual anomers of O-methylated lactose is compelling and allows us to assign peaks 1 and 2 in the ATD of LNnT (Figure 2a) to the β- and α-anomers, respectively. We can then add the anomer-specific IR spectra of both lactose and LNnT (Figure S2) to a spectroscopic database for analyzing human milk oligosaccharides.

Maltopentaose. To investigate how this procedure can be used to analyze a reducing sugar that features a more complex ATD, we investigated the different drift peaks of maltopentaose, which is commonly used in the preparation of dextran ladders for capillary electrophoreses.[52] The ATD obtained after three IMS cycles is displayed in Figure 3a and contains four

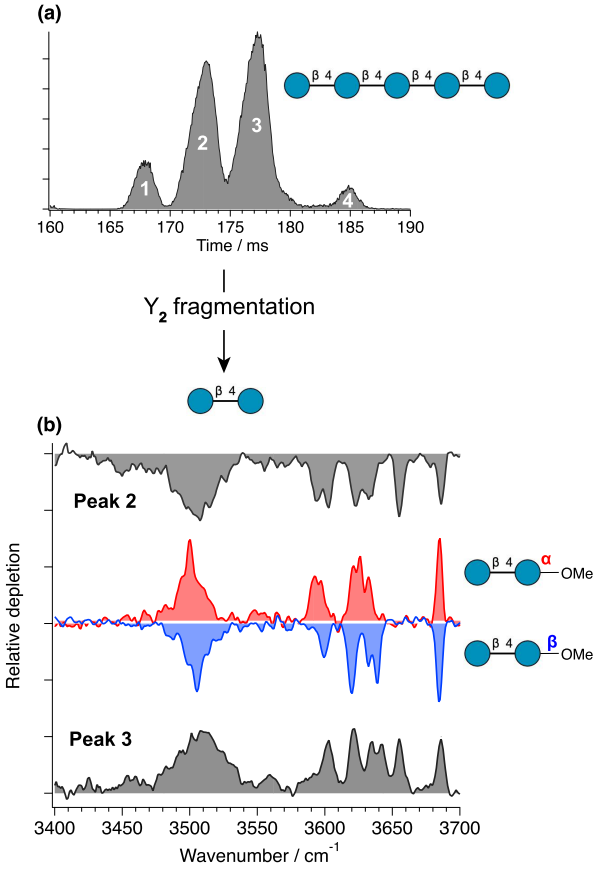

Figure 3. (a) Arrival-time distribution of sodiated maltopentaose, which separates into four species after three IM separation cycles (31 m drift path). (b) Comparison of the cryogenic vibrational spectra of the Y_2-fragments from the second and third mobility peaks with those of methyl-α-maltosidase and methyl-β-maltosidase.

well-separated peaks. Similar results were observed in previous high-resolution IMS studies, and it has been speculated that the two major peaks originate from the reducing-end anomers, while the other structures may represent open-ring configurations.[29,53]

To investigate the identity of the separated species, we produced the Y_2-fragment (corresponding to maltose) from each peak in the ATD and compared the spectra of these fragments to those of the anomerically pure methyl-α-maltosidase and methyl-β-maltosidase. Since the Y_2-fragment is isomeric to the C_2-fragment in this molecule, a separate experiment was performed on a Waters QToF Premier, in which we labeled the reducing end with ^{18}O in order to distinguish between these two fragment types. The tandem mass spectra (Figure S3) showed that the Y_2-fragment is preferentially formed over the C_2-fragment. Assuming similar dissociation propensities during the CID process on our spectroscopy instrument, we expect to observe predominantly the Y_2-fragment species there as well. Upon comparing the spectra of the fragments from the two major drift peaks to the anomerically pure methylated standards (Figure 3b), we find that a transition at 3655 cm^{-1} is missing in the spectra of both O-methylated standards, which can be assigned to the anomeric OH stretch vibration. Other small differences between the spectra of the Y_2-fragments and the O-methylated standards, such as the shape of the low-frequency band around 3510 cm^{-1}, can be attributed to a change in the hydrogen-bonding network upon removal of one OH oscillator. Despite these slight differences, we can match the fragment from peak 2 to the methylated α-anomer and the fragment from peak 3 to that of the methylated β-anomer. This further illustrates the sensitivity of IR spectroscopy to the slightest change in molecular structure.

We can thus assign the two major peaks in the ATD of maltopentaose to the reducing-end anomers. The spectra of the Y_2-fragments from peaks 1 and 4 resemble each other (Figure S4); however, they do not show any resemblance to the O-methylated standards and must therefore correspond to some other conformations at the reducing end, such as an open-ring form, as proposed previously,[53] or a furanose ring.[54]

CONCLUSIONS

In this work, we have demonstrated how the combination of ion-mobility-selective CID with cryogenic IR spectroscopy can be used to identify the reducing-end anomers of biologically relevant oligosaccharides. By exploiting the fact that Y-fragments retain the anomeric information on their precursor structures, we are able to identify the mobility-separated anomers of larger glycans by spectroscopically matching their fragments to anomerically pure, commercially available mono- and disaccharides or those selectively formed by C-fragments that retain the anomericity of the glycosidic bond.

This method also allows us to obtain the anomerically pure IR fingerprints of large molecules for which methylated standards are often not obtainable. These fingerprints can in turn be used as standards to assign structures of still larger, more complex oligosaccharides as we have demonstrated in a recent publication.[41] Ultimately, a sufficiently large database can be created, allowing for rapid structural identification of large, unknown oligosaccharides.

More broadly, the general approach employed here can be used to identify the other types of CID fragments, which will help in piecing together the primary structure of isomerically complex glycans.

ASSOCIATED CONTENT

Supporting Information

The Supporting Information is available free of charge at https://pubs.acs.org/doi/10.1021/jasms.2c00043.

Vibrational spectra of precursor glycans associated with Figures 1−3 and tandem mass spectrum of ^{18}O-labeled [maltopentaose]Na^+ (PDF)

https://doi.org/10.1021/jasms.2c00043
J. Am. Soc. Mass Spectrom. 2022, 33, 859−864

AUTHOR INFORMATION

Corresponding Author

Thomas R. Rizzo − *Laboratoire de Chimie Physique Moléculaire, EPFL SB ISIC LCPM, École Polytechnique Fédérale de Lausanne, CH-1015 Lausanne, Switzerland;* orcid.org/0000-0003-2796-905X; Email: thomas.rizzo@epfl.ch

Authors

Robert P. Pellegrinelli − *Laboratoire de Chimie Physique Moléculaire, EPFL SB ISIC LCPM, École Polytechnique Fédérale de Lausanne, CH-1015 Lausanne, Switzerland*

Lei Yue − *Laboratoire de Chimie Physique Moléculaire, EPFL SB ISIC LCPM, École Polytechnique Fédérale de Lausanne, CH-1015 Lausanne, Switzerland*

Eduardo Carrascosa − *Laboratoire de Chimie Physique Moléculaire, EPFL SB ISIC LCPM, École Polytechnique Fédérale de Lausanne, CH-1015 Lausanne, Switzerland;* orcid.org/0000-0003-4338-8669

Ahmed Ben Faleh − *Laboratoire de Chimie Physique Moléculaire, EPFL SB ISIC LCPM, École Polytechnique Fédérale de Lausanne, CH-1015 Lausanne, Switzerland;* orcid.org/0000-0002-9144-2052

Stephan Warnke − *Laboratoire de Chimie Physique Moléculaire, EPFL SB ISIC LCPM, École Polytechnique Fédérale de Lausanne, CH-1015 Lausanne, Switzerland;* orcid.org/0000-0001-7481-286X

Priyanka Bansal − *Laboratoire de Chimie Physique Moléculaire, EPFL SB ISIC LCPM, École Polytechnique Fédérale de Lausanne, CH-1015 Lausanne, Switzerland*

Complete contact information is available at: https://pubs.acs.org/10.1021/jasms.2c00043

Notes

The authors declare no competing financial interest.

ACKNOWLEDGMENTS

The authors thank the Swiss National Science Foundation through grants 200020_184838 and 206021_177004, the European Research Council (Grant 788697-GLYCANAL), and the EPFL for the financial support of this work.

REFERENCES

(1) Varki, A. Biological roles of glycans. *Glycobiology* **2017**, *27*, 3−49.

(2) Cummings, R. D.; Pierce, J. M. The Challenge and Promise of Glycomics. *Chem. Biol.* **2014**, *21* (1), 1−15.

(3) Rudd, P. M.; Elliott, T.; Cresswell, P.; Wilson, I. A.; Dwek, R. A. Glycosylation and the Immune System. *Science* **2001**, *291* (5512), 2370−2376.

(4) Shajahan, A.; Supekar, N. T.; Gleinich, A. S.; Azadi, P. Deducing the N- and O-glycosylation profile of the spike protein of novel coronavirus SARS-CoV-2. *Glycobiology* **2020**, *30* (12), 981−988.

(5) Walls, A. C.; Park, Y.-J.; Tortorici, M. A.; Wall, A.; McGuire, A. T.; Veesler, D. Structure, Function, and Antigenicity of the SARS-CoV-2 Spike Glycoprotein. *Cell* **2020**, *181* (2), 281−292.e6.

(6) Rossen, J. W. A.; de Beer, R.; Godeke, G. J.; Raamsman, M. J. B.; Horzinek, M. C.; Vennema, H.; Rottier, P. J. M. The Viral Spike Protein Is Not Involved in the Polarized Sorting of Coronaviruses in Epithelial Cells. *J. Virol.* **1998**, *72* (1), 497−503.

(7) Pallesen, J.; Wang, N.; Corbett, K. S.; Wrapp, D.; Kirchdoerfer, R. N.; Turner, H. L.; Cottrell, C. A.; Becker, M. M.; Wang, L.; Shi, W.; Kong, W.-P.; Andres, E. L.; Kettenbach, A. N.; Denison, M. R.; Chappell, J. D.; Graham, B. S.; Ward, A. B.; McLellan, J. S. Immunogenicity and structures of a rationally designed prefusion MERS-CoV spike antigen. *Proc. Natl. Acad. Sci. U.S.A.* **2017**, *114* (35), E7348−E7357.

(8) Vigerust, D. J.; Shepherd, V. L. Virus glycosylation: role in virulence and immune interactions. *Trends Microbiol.* **2007**, *15* (5), 211−218.

(9) Roberts, D. S.; Mann, M.; Melby, J. A.; Larson, E. J.; Zhu, Y.; Brasier, A. R.; Jin, S.; Ge, Y. Structural O-Glycoform Heterogeneity of the SARS-CoV-2 Spike Protein Receptor-Binding Domain Revealed by Top-Down Mass Spectrometry. *J. Am. Chem. Soc.* **2021**, *143* (31), 12014−12024.

(10) Harvey, D. J. Collision-induced fragmentation of underivatized N-linked carbohydrates ionized by electrospray. *J. Mass Spectrom.* **2000**, *35* (10), 1178−1190.

(11) Mechref, Y.; Novotny, M. V.; Krishnan, C. Structural Characterization of Oligosaccharides Using Maldi-TOF/TOF Tandem Mass Spectrometry. *Anal. Chem.* **2003**, *75* (18), 4895−4903.

(12) An, H. J.; Lebrilla, C. B. Structure elucidation of native N- and O-linked glycans by tandem mass spectrometry (tutorial). *Mass Spectrom. Rev.* **2011**, *30* (4), 560−578.

(13) Harvey, D. J.; Royle, L.; Radcliffe, C. M.; Rudd, P. M.; Dwek, R. A. Structural and quantitative analysis of N-linked glycans by matrix-assisted laser desorption ionization and negative ion nanospray mass spectrometry. *Anal. Biochem.* **2008**, *376* (1), 44−60.

(14) Gaucher, S. P.; Leary, J. A. Determining anomericity of the glycosidic bond in Zn(II)-diethylenetriamine-disaccharide complexes using MSnin a quadrupole ion trap. *J. Am. Soc. Mass Spectrom.* **1999**, *10* (3), 269−272.

(15) Tsai, S.-T.; Liew, C. Y.; Hsu, C.; Huang, S.-P.; Weng, W.-C.; Kuo, Y.-H.; Ni, C.-K. Automatic Full Glycan Structural Determination through Logically Derived Sequence Tandem Mass Spectrometry. *ChemBioChem.* **2019**, *20* (18), 2351−2359.

(16) Liew, C. Y.; Yen, C.-C.; Chen, J.-L.; Tsai, S.-T.; Pawar, S.; Wu, C.-Y.; Ni, C.-K. Structural identification of N-glycan isomers using logically derived sequence tandem mass spectrometry. *Commun. Chem.* **2021**, *4* (1), 92.

(17) Welply, J. K. Sequencing methods for carbohydrates and their biological applications. *Trends Biotechnol.* **1989**, *7* (1), 5−10.

(18) Morelle, W.; Michalski, J.-C. Analysis of protein glycosylation by mass spectrometry. *Nat. Protoc.* **2007**, *2* (7), 1585−1602.

(19) Mariño, K.; Bones, J.; Kattla, J. J.; Rudd, P. M. A systematic approach to protein glycosylation analysis: a path through the maze. *Nat. Chem. Biol.* **2010**, *6* (10), 713−723.

(20) Liu, Y.; Clemmer, D. E. Characterizing Oligosaccharides Using Injected-Ion Mobility/Mass Spectrometry. *Anal. Chem.* **1997**, *69* (13), 2504−2509.

(21) Hofmann, J.; Stuckmann, A.; Crispin, M.; Harvey, D. J.; Pagel, K.; Struwe, W. B. Identification of Lewis and Blood Group Carbohydrate Epitopes by Ion Mobility-Tandem-Mass Spectrometry Fingerprinting. *Anal. Chem.* **2017**, *89* (4), 2318−2325.

(22) Hofmann, J.; Pagel, K. Glycan Analysis by Ion Mobility-Mass Spectrometry. *Angew. Chem., Int. Ed.* **2017**, *56* (29), 8342−8349.

(23) Gray, C. J.; Schindler, B.; Migas, L. G.; Pičmanová, M.; Allouche, A. R.; Green, A. P.; Mandal, S.; Motawia, M. S.; Sánchez-Pérez, R.; Bjarnholt, N.; Møller, B. L.; Rijs, A. M.; Barran, P. E.; Compagnon, I.; Eyers, C. E.; Flitsch, S. L. Bottom-Up Elucidation of Glycosidic Bond Stereochemistry. *Anal. Chem.* **2017**, *89* (8), 4540−4549.

(24) Mookherjee, A.; Uppal, S. S.; Murphree, T. A.; Guttman, M. Linkage Memory in Underivatized Protonated Carbohydrates. *J. Am. Soc. Mass Spectrom.* **2021**, *32*, 581.

(25) Hamid, A. M.; Ibrahim, Y. M.; Garimella, S. V. B.; Webb, I. K.; Deng, L.; Chen, T.-C.; Anderson, G. A.; Prost, S. A.; Norheim, R. V.; Tolmachev, A. V.; Smith, R. D. Characterization of Traveling Wave Ion Mobility Separations in Structures for Lossless Ion Manipulations. *Anal. Chem.* **2015**, *87* (22), 11301−11308.

(26) Deng, L.; Ibrahim, Y. M.; Hamid, A. M.; Garimella, S. V. B.; Webb, I. K.; Zheng, X.; Prost, S. A.; Sandoval, J. A.; Norheim, R. V.; Anderson, G. A.; Tolmachev, A. V.; Baker, E. S.; Smith, R. D. Ultra-High Resolution Ion Mobility Separations Utilizing Traveling Waves

in a 13 m Serpentine Path Length Structures for Lossless Ion Manipulations Module. *Anal. Chem.* **2016**, *88* (18), 8957−8964.
(27) Nagy, G.; Attah, I. K.; Garimella, S. V. B.; Tang, K.; Ibrahim, Y. M.; Baker, E. S.; Smith, R. D. Unraveling the isomeric heterogeneity of glycans: ion mobility separations in structures for lossless ion manipulations. *Chem. Commun.* **2018**, *54* (83), 11701−11704.
(28) Giles, K.; Ujma, J.; Wildgoose, J.; Pringle, S.; Richardson, K.; Langridge, D.; Green, M. A Cyclic Ion Mobility-Mass Spectrometry System. *Anal. Chem.* **2019**, *91* (13), 8564−8573.
(29) Ujma, J.; Ropartz, D.; Giles, K.; Richardson, K.; Langridge, D.; Wildgoose, J.; Green, M.; Pringle, S. Cyclic Ion Mobility Mass Spectrometry Distinguishes Anomers and Open-Ring Forms of Pentasaccharides. *J. Am. Soc. Mass Spectrom.* **2019**, *30* (6), 1028−1037.
(30) Hollerbach, A. L.; Li, A.; Prabhakaran, A.; Nagy, G.; Harrilal, C. P.; Conant, C. R.; Norheim, R. V.; Schimelfenig, C. E.; Anderson, G. A.; Garimella, S. V. B.; Smith, R. D.; Ibrahim, Y. M. Ultra-High-Resolution Ion Mobility Separations Over Extended Path Lengths and Mobility Ranges Achieved using a Multilevel Structures for Lossless Ion Manipulations Module. *Anal. Chem.* **2020**, *92* (11), 7972−7979.
(31) Schindler, B.; Barnes, L.; Renois, G.; Gray, C.; Chambert, S.; Fort, S.; Flitsch, S.; Loison, C.; Allouche, A.-R.; Compagnon, I. Anomeric memory of the glycosidic bond upon fragmentation and its consequences for carbohydrate sequencing. *Nat. Commun.* **2017**, *8* (1), 973.
(32) Gray, C. J.; Compagnon, I.; Flitsch, S. L. Mass spectrometry hybridized with gas-phase InfraRed spectroscopy for glycan sequencing. *Curr. Opin. Struct. Biol.* **2020**, *62*, 121−131.
(33) Mucha, E.; González Flórez, A. I.; Marianski, M.; Thomas, D. A.; Hoffmann, W.; Struwe, W. B.; Hahm, H. S.; Gewinner, S.; Schöllkopf, W.; Seeberger, P. H.; von Helden, G.; Pagel, K. Glycan Fingerprinting via Cold-Ion Infrared Spectroscopy. *Angew. Chem., Int. Ed.* **2017**, *56* (37), 11248−11251.
(34) Khanal, N.; Masellis, C.; Kamrath, M. Z.; Clemmer, D. E.; Rizzo, T. R. Cryogenic IR spectroscopy combined with ion mobility spectrometry for the analysis of human milk oligosaccharides. *Analyst* **2018**, *143* (8), 1846−1852.
(35) Masellis, C.; Khanal, N.; Kamrath, M. Z.; Clemmer, D. E.; Rizzo, T. R. Cryogenic Vibrational Spectroscopy Provides Unique Fingerprints for Glycan Identification. *J. Am. Soc. Mass Spectrom.* **2017**, *28* (10), 2217−2222.
(36) Ben Faleh, A.; Warnke, S.; Rizzo, T. R. Combining Ultrahigh-Resolution Ion-Mobility Spectrometry with Cryogenic Infrared Spectroscopy for the Analysis of Glycan Mixtures. *Anal. Chem.* **2019**, *91* (7), 4876−4882.
(37) Warnke, S.; Ben Faleh, A.; Pellegrinelli, R. P.; Yalovenko, N.; Rizzo, T. R. Combining ultra-high resolution ion mobility spectrometry with cryogenic IR spectroscopy for the study of biomolecular ions. *Faraday Discuss.* **2019**, *217*, 114−125.
(38) Dyukova, I.; Ben Faleh, A.; Warnke, S.; Yalovenko, N.; Yatsyna, V.; Bansal, P.; Rizzo, T. R. A new approach for identifying positional isomers of glycans cleaved from monoclonal antibodies. *Analyst* **2021**, *146* (15), 4789−4795.
(39) Rizzo, T. R.; Boyarkin, O. V. Cryogenic Methods for the Spectroscopy of Large, Biomolecular Ions. *Gas-Phase IR Spectroscopy and Structure of Biological Molecules* **2014**, *364*, 43−97.
(40) Yalovenko, N.; Yatsyna, V.; Bansal, P. H.; AbiKhodr, A. R.; Rizzo, T. Analyzing glycans cleaved from a biotherapeutic protein using ultrahigh-resolution ion mobility spectrometry together with cryogenic ion spectroscopy. *Analyst* **2020**, *145* (20), 6493−6499.
(41) Bansal, P.; Ben Faleh, A.; Warnke, S.; Rizzo, T. R. Identification of N-glycan positional isomers by combining IMS and vibrational fingerprinting of structurally determinant CID fragments. *Analyst* **2022**, *147*, 704.
(42) Barnes, L.; Schindler, B.; Chambert, S.; Allouche, A.-R.; Compagnon, I. Conformational preferences of protonated N-acetylated hexosamines probed by InfraRed Multiple Photon Dissociation (IRMPD) spectroscopy and ab initio calculations. *Int. J. Mass spectrom.* **2017**, *421*, 116−123.
(43) Barnes, L.; Allouche, A.-R.; Chambert, S.; Schindler, B.; Compagnon, I. Ion spectroscopy of heterogeneous mixtures: IRMPD and DFT analysis of anomers and conformers of monosaccharides. *Int. J. Mass spectrom.* **2020**, *447*, 116235.
(44) Domon, B.; Costello, C. E. A systematic nomenclature for carbohydrate fragmentations in FAB-MS/MS spectra of glycoconjugates. *Glycoconjugate J.* **1988**, *5* (4), 397−409.
(45) Bansal, P.; Yatsyna, V.; AbiKhodr, A. H.; Warnke, S.; Ben Faleh, A.; Yalovenko, N.; Wysocki, V. H.; Rizzo, T. R. Using SLIM-Based IMS-IMS Together with Cryogenic Infrared Spectroscopy for Glycan Analysis. *Anal. Chem.* **2020**, *92* (13), 9079−9085.
(46) Pellegrinelli, R. P.; Yue, L.; Carrascosa, E.; Warnke, S.; Ben Faleh, A.; Rizzo, T. R. How General Is Anomeric Retention during Collision-Induced Dissociation of Glycans? *J. Am. Chem. Soc.* **2020**, *142* (13), 5948−5951.
(47) Warnke, S.; Ben Faleh, A.; Rizzo, T. R. Toward High-Throughput Cryogenic IR Fingerprinting of Mobility-Separated Glycan Isomers. *ACS Meas. Sci. Au* **2021**, *1*, 157.
(48) Webb, I. K.; Garimella, S. V. B.; Tolmachev, A. V.; Chen, T.-C.; Zhang, X.; Norheim, R. V.; Prost, S. A.; LaMarche, B.; Anderson, G. A.; Ibrahim, Y. M.; Smith, R. D. Experimental Evaluation and Optimization of Structures for Lossless Ion Manipulations for Ion Mobility Spectrometry with Time-of-Flight Mass Spectrometry. *Anal. Chem.* **2014**, *86* (18), 9169−9176.
(49) Hamid, A. M.; Garimella, S. V. B.; Ibrahim, Y. M.; Deng, L.; Zheng, X.; Webb, I. K.; Anderson, G. A.; Prost, S. A.; Norheim, R. V.; Tolmachev, A. V.; Baker, E. S.; Smith, R. D. Achieving High Resolution Ion Mobility Separations Using Traveling Waves in Compact Multiturn Structures for Lossless Ion Manipulations. *Anal. Chem.* **2016**, *88* (18), 8949−8956.
(50) Brockhausen, I.; Stanley, P. O-GalNAc Glycans. In *Essentials of Glycobiology*, 3rd ed.; Varki, A., Cummings, R. D., Esko, J. D., Stanley, P., Hart, G. W., Aebi, M., Darvill, A. G., Kinoshita, T., Packer, N. H., Prestegard, J. H., Schnaar, R. L., Seeberger, P. H., Eds.; Cold Spring Harbor Laboratory Press: Cold Spring Harbor, NY, 2017.
(51) Warnke, S.; Ben Faleh, A.; Scutelnic, V.; Rizzo, T. R. Separation and Identification of Glycan Anomers Using Ultrahigh-Resolution Ion-Mobility Spectrometry and Cryogenic Ion Spectroscopy. *J. Am. Soc. Mass Spectrom.* **2019**, *30* (11), 2204−2211.
(52) Partyka, J.; Foret, F. Cationic labeling of oligosaccharides for electrophoretic preconcentration and separation with contactless conductivity detection. *J. Chromatogr. A* **2012**, *1267*, 116−120.
(53) Deng, L.; Ibrahim, Y. M.; Baker, E. S.; Aly, N. A.; Hamid, A. M.; Zhang, X.; Zheng, X.; Garimella, S. V. B.; Webb, I. K.; Prost, S. A.; Sandoval, J. A.; Norheim, R. V.; Anderson, G. A.; Tolmachev, A. V.; Smith, R. D. Ion Mobility Separations of Isomers based upon Long Path Length Structures for Lossless Ion Manipulations Combined with Mass Spectrometry. *ChemistrySelect* **2016**, *1* (10), 2396−2399.
(54) Ho, J. S.; Gharbi, A.; Schindler, B.; Yeni, O.; Brédy, R.; Legentil, L.; Ferrières, V.; Kiessling, L. L.; Compagnon, I. Distinguishing Galactoside Isomers with Mass Spectrometry and Gas-Phase Infrared Spectroscopy. *J. Am. Chem. Soc.* **2021**, *143* (28), 10509−10513.

https://doi.org/10.1021/jasms.2c00043
J. Am. Soc. Mass Spectrom. 2022, 33, 859−864